Effects of the RGTFEGKF Inhibitor on the Structures of the Transmembrane Fragment 70−86 of Glycophorin A: An All-Atom Molecular Dynamics Study

Huiyu Li,[†] Yin Luo,[†] Philippe Derreumaux,[‡] and Guanghong Wei*,[†]

Surface Physics Laboratory (National Key Laboratory) and Department of Physics, Fudan University, 220 Handan Road, Shanghai, 200433, People's Republic of China and Laboratoire de Biochimie Théorique, UPR 9080 CNRS, Institut de Biologie Physico−Chimique et Université Paris Diderot, Paris 7, 13 rue Pierre et Marie Curie, 75005 Paris, France

Received: September 14, 2009; Revised Manuscript Received: December 4, 2009

There is experimental evidence that the transmembrane fragment spanning amino acids 70−86 of glycophorin A, GpA70−86, forms amyloid fibrils and the inhibitor RGTFEGKF prevents GpA70−86 fibril formation at an equimolar ratio. Both the GpA70−86 and inhibitor peptides contain a GxxxG motif as found in many amyloid proteins such as the Alzheimer's amyloid β-peptide and prion protein. To explore the intrinsic, early interaction and inhibition mechanism, we have determined the structures of GpA70−86 in the absence and presence of the inhibitor by means of extensive molecular dynamics simulations in explicit solvent. Consistent with experiments on the fibrils, our simulations show that the two GxxxG motifs interact significantly at the monomer level. They go, however, one step beyond by indicating that the inhibitor has a significant impact on the global structure of GpA70−86, but a limited influence on the conformations of the GxxxG motif. Implications of our simulations on amyloid propagation of proteins containing GxxxG motifs are discussed.

Introduction

Amyloid fibrils associated with neurodegenerative diseases such as Alzheimer's are often derived from the transmembrane helices of proteins. It is known that all fibrils contain a common cross β-sheet structure with β-strands perpendicular and hydrogen bonds parallel to the fibril axis.[1] Within the amyloid-β peptide (Aβ) sequence, there are three consecutive repeats of a GxxxG motif, which may be involved in both peptide aggregation and membrane perturbation, processes that have been implicated in oligomer toxicity leading to Alzheimer's disease.[2,3] This GxxxG motif is also detected three times in the prion protein within amino acids 113−135[4,5] and one time in the α-synuclein protein within amino acids 63−85,[6] associated with Creutzfeld−Jacob's and Parkinson's diseases, respectively.

To investigate the role of glycine in amyloid fibrils formed from transmembrane proteins, Smith et al. studied a model peptide corresponding to the single transmembrane helix of glycophorin A, spanning residues 70−86 (GpA70−86) by FTIR, solid-state NMR and fluorescence spectroscopies and electron microscopy.[7] This peptide contains a GxxxG motif between positions 79 and 83. This study showed that GpA70−86 peptides adopt almost exclusively β-sheet structure immediately following reconstruction with lipid bilayers, and associate into amyloid fibrils with in-register, parallel orientation of the β-strands after 3 days in aqueous solution. This in-register parallel orientation, observed for other amyloids,[8−10] allows the amino acids with large side chains to form complementary molecular ridges that can pack into the glycine grooves.[7] On the basis of these findings, they successfully designed an 8-residue peptide containing a GxxxG motif that targets the glycine grooves and destabilizes GpA70−86 fibril formation. By using 2D NMR spectra, they showed that the inhibitor disrupts the intermolecular Gly79-Met81 contact at a 1:1 molar ratio of inhibitor to GpA70−86 peptide.

Although intermolecular GxxxG interactions either stabilize sheet-to-sheet packing in fibrils or drive fibril disassembly when GpA70−86 is incubated with a GxxxG inhibitor,[7] the first step of the interaction mechanism between GpA70−86 and the inhibitor at the monomer level remains to be determined. While coarse-grained protein simulations in implicit aqueous solution accelerate sampling of conformational space,[11,12] we here use the full atomic representation of the peptides and water molecules. By performing extensive molecular dynamics (MD) simulations for each compound and the complex, we find that the intermolecular GxxxG interactions are essential in the recognition process at the monomer level, thereby confirming solid-state 2D NMR experiments conducted at an equimolar mixture. Moreover, our simulations provide strong evidence that the conformations of the GxxxG motif in GpA70−86 are mostly unaffected by the inhibitor, offering the view that this motif spends most of its time in an extended state.

Materials and Methods

The sequence of GpA70−86 peptide is EPEITLIIFGVMAGWIG and that of the 8-residue inhibitor is RGTFEGKF-NH2. To mimic the experimental neutral pH condition, the side-chains of Arg, Lys, and Glu are charged (Arg^+, Lys^+, Glu^-), the N- and C-termini (NH_3^+, COO^-) of GpA70−86 and the N-terminal (NH^{3+}) of the inhibitor are also charged.

MD Simulations. All of the simulations are performed using the GROMACS software package[13] and GROMOS96 force field.[14] Water is modeled by the explicit simple point charge (SPC) model.[15] The LINCS[16] and SETTLE[17] algorithms are used to constrain the bond lengths within peptide and water mol-

* To whom correspondence should be addressed. Department of Physics, Fudan University, 220 Handan Road, Shanghai, 200433, People's Republic of China. Tel: (86) 21 55665231. Fax: (86) 21 65104949. E-mail: ghwei@fudan.edu.cn.

† Surface Physics Laboratory (National Key Laboratory) and Department of Physics, Fudan University.

‡ Laboratoire de Biochimie Théorique, UPR 9080 CNRS, Institut de Biologie Physico−Chimique et Université Paris Diderot.

10.1021/jp908889q
Published on Web 12/29/2009

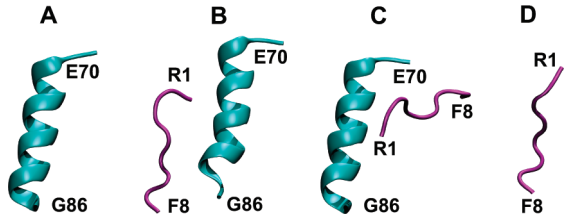

Figure 1. The initial states of MD runs: (A) for the isolated GpA70−86 peptide; (B, C) for the GpA70−86-inhibitor complex, and (D) for the isolated inhibitor. The minimal interpeptide distance is 0.65 nm between Met81 and Phe4 in (B) and 0.39 nm between Val84 and Phe8 in (C).

ecules, respectively. This allows an integration time step of 2 fs. A twin-range cutoff 1.0/1.4 nm is used for the nonbonded interactions, and a reaction-field correction with dielectric permittivity $\varepsilon = 78$ is employed to calculate long-range electrostatics interactions. The solute and solvent are separately coupled to external temperature and pressure baths. The temperature is maintained close to 310 K by weak coupling to an external temperature bath[18] with a coupling constant of 0.1 ps, and the pressure is kept at 1 bar using a coupling time of 1.0 ps. All MD simulations are performed using periodic boundary conditions in a truncated octahedron box. For the systems of isolated GpA, inhibitor, and fibril model, the minimum distance between the peptide and the water box wall is 1.2 nm. For the GpA−inhibitor complex, the minimum distance is 1.5 nm, which provides large space to allow the inhibitor to move around the GpA70−86 peptide.

Isolated GpA70−86/Inhibitor. The starting MD point for GpA70−86 in Figure 1A with α-helical character is taken from its conformation within the dimer structure of GpA70−98 (pdb ID: 1afo).[19] The starting MD structure for the inhibitor in Figure 1D is extended. The total number of atoms is around 10 000 and 6500 in the GpA70−86 and inhibitor simulations, respectively.

GpA70−86−Inhibitor Complex. We construct two distinct starting MD points using the α-helical state of GpA70−86 and an extended conformation of the inhibitor. The inhibitor is either parallel to GpA70−86 (Figure 1B) or in a randomly chosen orientation (Figure 1C). The C_α-root-mean-square deviation (rmsd) between the two states is 7.8 Å. The total number of atoms is around 15 000.

GpA70−86 Fibril Model. On the basis of the equilibrium ensemble of GpA70−86 in aqueous solution, we construct an amyloid cross-β-structure consisting of 12 peptide chains in β-strand−loop−β-strand conformations and satisfying solid-state NMR distances as described below. The total number of atoms is around 11 500.

Analysis. The trajectories of all nonfibril models are analyzed using several order parameters. These include the probability distributions of the C_α end-to-end and G-to-G distances, and the secondary structure content using the DSSP program.[20] The MD-generated structures of the GpA70−86 and GpA70−86-inhibitor systems are clustered using a C_α-rmsd cutoff of 0.28 nm. The interactions in the GpA70−86-inhibitor complex are analyzed by the probability of main-chain−main-chain and side-chain−side-chain contact maps. Here, a contact is defined when aliphatic carbon atoms of two nonsequential side-chains (or main-chains) come within 0.54 nm or any other atom of two nonsequential side-chains (or main-chains) lies within 0.46 nm.[21] We also cluster the GxxxG conformations in each system using a C_α-rmsd cutoff of 0.07 nm. Unless specified, the data used in the analysis are within 100−300 ns MD simulations. The stability of the constructed fibril model is analyzed by the C_α-rmsd with respect to its initial minimized structure and two order parameters as a function of time. All representations are drawn using VMD program.[22]

TABLE 1: Setup Details of All Simulations, Each of 300 ns, at 310 K[a]

system	no. of MD runs	initial state
GpA	5	Figure 1A
GpA−inhibitor	2	Figure 1B
GpA−inhibitor	6	Figure 1C
inhibitor	2	Figure 1D

[a] For each system, we describe the number of runs and the starting state. For brevity, we use GpA for GpA70-86.

Results

To characterize the structures of the isolated GpA70−86, isolated inhibitor, and the GpA70−86-inhibitor complex, a total of 5, 2, and 8 MD runs, each of 300 ns, are carried out, respectively. A summary of the MD setup details is given in Table 1. All runs use different initial velocity distributions. The first 100 ns of each run are discarded in the analysis to remove the bias of the initial states. The conformational properties are therefore based on 1, 0.4, and 1.6 μs for the GpA70−86, 8-residue inhibitor and the complex, respectively.

The convergence of the MD simulations is demonstrated by comparing the C_α end-to-end distance distributions of each chain either in isolation (Figures 2A,B) or in the complex (Figures 2C,D) using 100−200 ns and 200−300 ns. As seen, the distributions are very similar using the two independent time intervals, with small differences in the profiles. This indicates that our simulations have reasonably converged at 310 K.

Differences in GpA70−86 conformations with and without the inhibitor are first characterized by structure cluster analysis. Using a C_α-rmsd cutoff of 0.28 nm, the centers of the first five most-populated clusters and their populations are shown in Figure 3. These clusters represent 30% and 32% of all GpA70−86 and GpA70−86-inhibitor conformations, respectively. For the isolated GpA70−86 peptide, the first four clusters shown in panel 3A display various β-hairpins, with Gly79 located at different positions in the turn and Gly83 mostly in β-sheet conformation. The fifth cluster is random coil. Within the complex, as seen in panel 3B, the GpA70−86 peptide displays random coil conformations (the first two clusters), a β-hairpin (the third cluster), and a helical fragment spanning Pro71-Phe78 (the fourth and fifth clusters).

The details of the interactions between the inhibitor and the GpA70−86 peptide are examined from the probability of main-chain−main-chain and side-chain−side-chain contacts. We see that the contact probability between the $G_{79}VMAG_{83}$ peptide motif and the G_2TFEG_6 inhibitor motif is the highest, with main-chain−main-chain interactions between Phe4 and Ala82-Gly83 being formed 50−60% of the time (Figure 4A) and the side-chain−side-chain contacts between Phe4 and Met81 being formed 30−40% of the time (Figure 4B). These contact maps with emphasis on the phenylalanine and methionine amino acids are consistent with the rational design of the inhibitor RGTFEGKF to target the GxxxG motif in GpA70−86 amyloid fibrils,[7] and phenylalanine promoting interaction of transmembrane domains via GxxxG motifs.[23]

The effect of the inhibitor on the GpA70−86 structures and the impact of GpA70−86 on the inhibitor structures can be further characterized by the end-to-end distance distribution of each chain (Figure 2). While a broad ensemble of states is

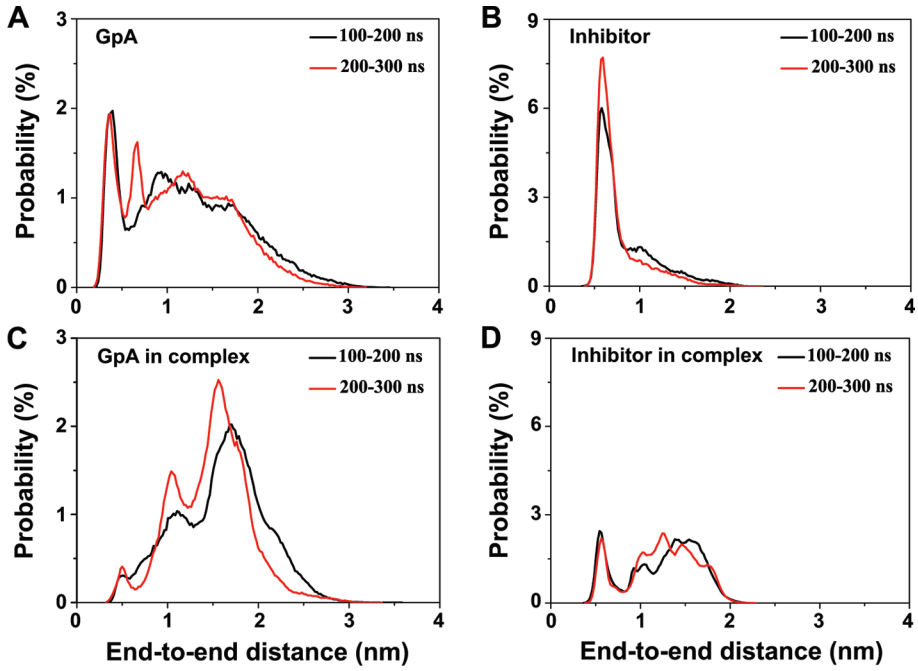

Figure 2. Probability distributions of C_α end-to-end distances for the GpA70−86 and inhibitor peptides within the time intervals 100−200 ns and 200−300 ns. GpA70−86 and the inhibitor in isolation (A and C) and in the complex (B and D).

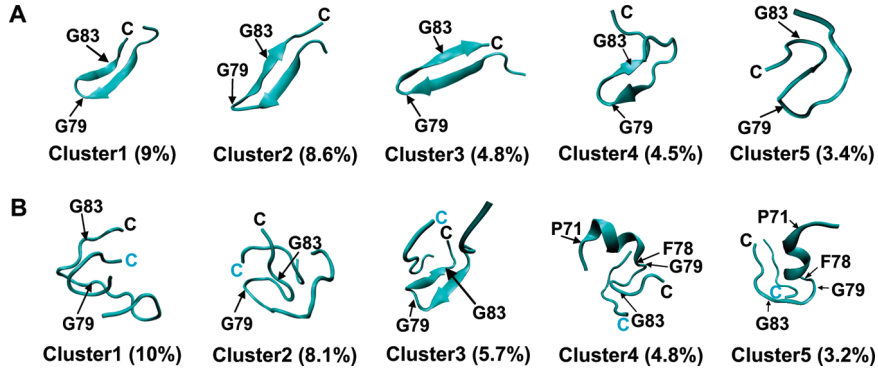

Figure 3. Equilibrium conformations of GpA70−86 and the GpA70−86-inhibitor complex. The center of the first five clusters using a C_α-rmsd cutoff of 0.28 nm for isolated GpA70−86 (A) and GpA70−86 with the inhibitor (B). The populations of these clusters are given in the parentheses. The C-terminus of each chain, and the location of the amino acids G79 and G83, are also indicated.

observed between 0.5 and 2.0 nm for the peptide in isolation (panel 2A), the ensemble shifts between 1.0 and 2.0 nm for the peptide within the complex (panel 2C). The inhibitor is also strongly affected with a dominant peak centered at 0.5 nm in isolated state (panel 2B) and a higher population of extended states in the complex (panel 2D).

The inhibitor also affects the secondary structure composition of GpA70−86 and vice versa. Overall, the GpA70−86 ordered secondary structure consists of 6% α-helix and 17% β-sheet in isolation vs 14% and 7% in the complex. Supporting Information Figure S1 shows that the N-terminal residues 72−76 of GpA70−86 have an averaged probability of 40% to display α-signal in the presence of inhibitor vs 20% when the inhibitor is absent. It is noted that the helical content of the C-terminal residues from Gly79 to Gly86 is 0%. In the presence of inhibitor, the percentage of β-sheet for residues 75−78 and 81−83 (10%) is much lower than that in the absence of inhibitor (30%). For the inhibitor, the β-sheet signal increases upon binding to GpA70−86 (see Figure S2 in Supporting Information). The region Thr3-Phe4-Glu5-Gly6 has an averaged β-sheet signal of 10% in the complex vs 0% when the inhibitor is isolated. Our cluster analysis calculation provides further evidence that this β-sheet signal mostly results from interactions with the GpA70−86 GxxxG motif.

The probability distributions of C_α Gly79-to-Gly83 and Gly2-to-Gly6 distances are shown in Figure 5. As expected from the end-to-end distance distribution using the full sequence, the GxxxG motif of the inhibitor is more extended in the complex than in isolation, with two peaks centered at 0.6 and 1.2 nm vs one peak at 0.6 nm, respectively (panel 5B). In contrast, the distance distribution for the GxxxG motif in GpA70−86 remains nearly the same in the absence and presence of inhibitor, with a strong preference for extended conformations (panel 5A). While the end-to-end distance for a canonical five-residue β-strand is 1.3 nm, we find that 60% and 46% of the GxxxG conformations have Gly79-to-Gly83 distances greater than 1.0 nm in isolated GpA70−86 and in the complex, respectively. The high similarity in the distance distribution is further evaluated by cluster analysis of all GxxxG conformations. We found that the centers of the first and second clusters in isolated GpA70−86 deviate from the centers of the first and second clusters of GpA70−86 in the complex by an averaged C_α-rmsd of 0.03 nm, indicating a structure conservation of GxxxG motif in the two different environments.

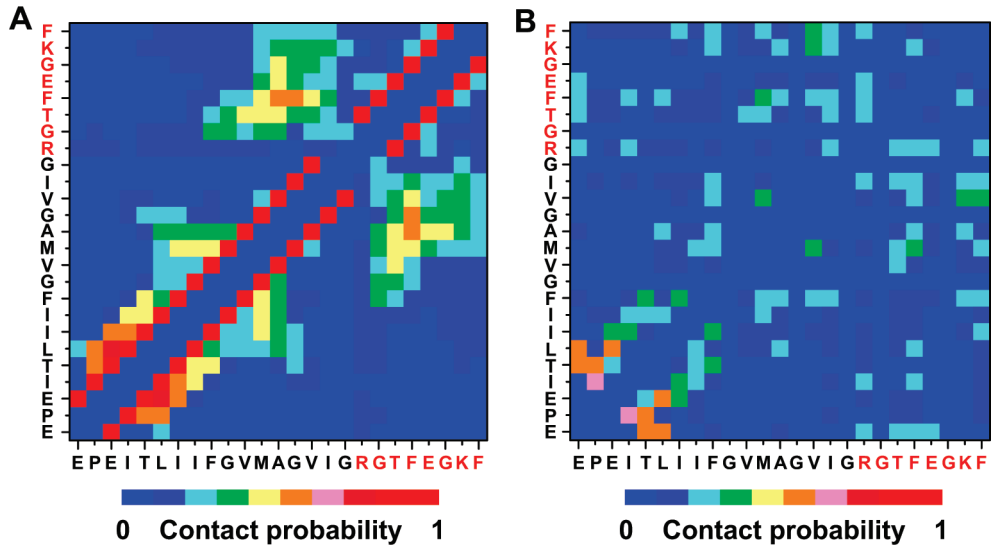

Figure 4. Contact map probability averaged over all 100−300 ns MD conformations of the GpA70−86-inhibitor complex for the (A) main-chain−main-chain and (B) side-chain−side-chain interactions.

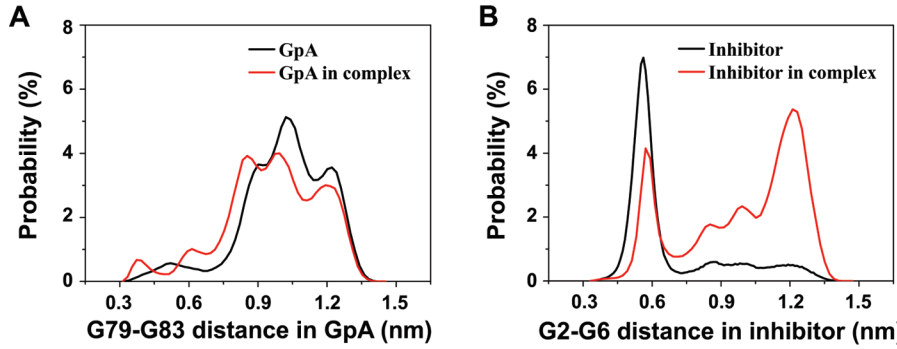

Figure 5. $C_\alpha-C_\alpha$ distance probability distribution of the GxxxG motif in (A) GpA in isolation and in the complex and (B) the inhibitor in isolation and in the complex.

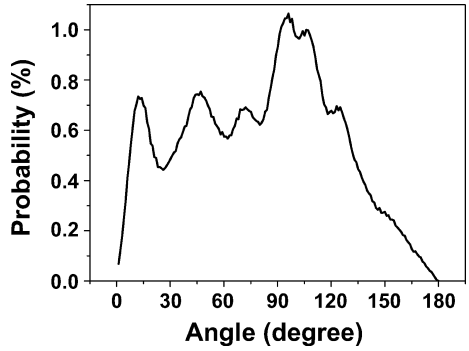

Figure 6. Distribution of the angle between vectors G79-G83 and G2-G6 in the GpA-inhibitor system.

To explore the orientation preference of the inhibitor with respect to GpA70−86, we plot in Figure 6 the probability distribution of the angle between the vectors Gly2-Gly6 and Gly79-Gly83. The probability peak at 90° indicates that the GxxxG motifs have a strong preference for perpendicular orientation. The peaks located at 15° and 45°, however, indicate that inhibitor also adopts parallel orientations relative to the GpA70−86. Besides these two orientations, the antiparallel configuration is also populated, albeit with a lower probability.

Discussion and Conclusions

The GxxxG motif has been the subject of many studies because of its importance in mediating helix−helix interactions in membrane proteins.[24,25] This motif is known to promote helix dimerization, but also trimerization of transmembrane proteins, although flanking and long-range amino acids modulate the affinity.[26] As a model system for the exploration of helix−helix interactions in integral membrane proteins, the glycophorin A helix has been often studied experimentally[27] and theoretically with coarse-grained or implicit membrane simulations by keeping the helices formed.[28−30]

It has been recently noted that the transmembrane fragment spanning amino acids 70−86 of glycophorin A, GpA70−86, forms amyloid fibrils in vitro and the inhibitor RGTFEGKF with a GxxxG motif prevents GpA70−86 fibril formation.[7] The GpA70−86 peptide is also very appealing for our understanding of Alzheimer's and Creutzfeld−Jacob's neurodegenerative diseases because it shares GxxxG motifs with the Aβ peptide and prion protein, respectively. There is strong experimental evidence that GxxxG motifs are critical for the etiology of Aβ42[3] and the substitution of Gly33 by Ala33 or Ile33 impacts Aβ42 oligomer distribution and toxicity.[2]

To investigate the early steps of the inhibitor RGTFEGKF on the conformations of GpA70−86 peptide at an experimental 1:1 molar ratio of peptide to inhibitor, we have determined the structures of the complex and each constituent by using extensive all-atom explicit solvent molecular dynamics simulations at physiological temperature. While the impact of inhibitors on preformed fibrils has already been discussed,[31−34] none of

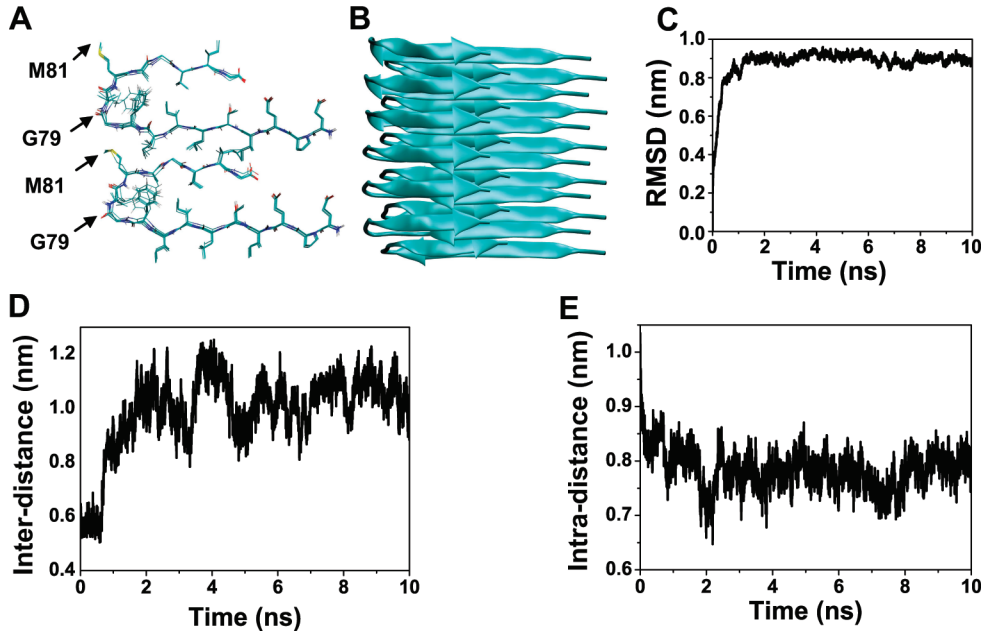

Figure 7. Analysis of the stability of a GpA70−86 fibril model consisting of 12 peptide chains, each with a strand-loop-strand conformation, an initial intermolecular Gly79(C)−Met81(CH3) distance of 0.3−0.5 nm and an intramolecular Gly79(C)−M81(CH3) distance of 0.8−1.0 nm. (A) Top view of the initial fibril model at an atomic level of representation with the positions of Gly79 and Met81 shown. (B) Side view of the fibril in cartoon representation; (C) Time evolution of the C_α-rmsd with respect to the initial model; (D) the intermolecular and (E) intramolecular NMR-derived distances. Similar properties are obtained from 5 runs using different random seeds.

them studied the intrinsic, early interaction and inhibition mechanism of inhibitor on the peptide using the experimental molar ratio.

Two factors can impact our results: the force field and the sampling. By using two peptides with α-helical and β-sheet characters, Yoda et al. found that GROMOS96 force field has a small bias for β-sheet structure in aqueous solution, while OPLS force field has not.[35] Recent replica exchange molecular dynamics studies on the β-amyloid peptide fragments Aβ(25−35) and Aβ(10−35) show, however, very similar results using GROMOS96 and OPLS/AA force fields.[36,37] Since the Aβ peptides, GpA70−86 and the inhibitor contain GxxxG motif, and all systems studied here are found to display little secondary structure, our equilibrium ensembles should not vary much by using another force field.

To provide further insights into the quality of the sampling of the inhibitor around the peptide, Figure S3 in Supporting Information shows, as a function of time, the angle between the vectors G2-G6 and G79-G83 and the peptide−inhibitor C_α PN-IN, PN-IC, PC-IN, and PC-IC distances (with P standing for GpA70−86, I for inhibitor, N for N-terminal C_α atom, and C for C-terminal C_α atom) for one run starting from the state shown in Figure 1C. Figure S3A of the Supporting Information reveals that the inhibitor explores many orientations around the peptide, ranging from parallel to antiparallel arrangements. Similarly, all C_α PN-IN, PN-IC, PC-IN, and PC-IC distances in Figure S3B of the Supporting Information fluctuate several times between 0.47 and 2.0 nm along the trajectory, indicating the extensive motion of the inhibitor around GpA70−86.

It is also of interest to check more starting structures of the inhibitor−peptide complex, where the two partners are not in contact at the beginning of the simulation. We therefore performed one additional 300-ns MD run starting from a complex shown in Figure S4A of the Supporting Information with a minimal interpeptide distance of 1.2 nm (namely between Glu70 and Phe4) and a minimum distance of 1.6 nm between the two GxxxG motifs. Figures S4B−D of the Supporting Information show the distributions of the four interpeptide terminal C_α−C_α distances by using our three distinct starting structures. We see that the three panels S4B−S4D share a dominant peak centered at 0.5 nm for the PC-IN distance, and the distributions in panels S4B and S4C overlap significantly, though starting from two very different positions and orientations of the inhibitor around the peptide. These results along with the high similarity of the distributions shown in Figure 2 using two independent time intervals demonstrate that our initial total of 8 simulations was sufficient to describe the equilibrium structures of the peptide−inhibitor complex.

Overall, our findings can be summarized as follows. First, our simulations show that the GpA70−86−inhibitor complex is essentially random coil in aqueous solution, but the two GxxxG motifs interact strongly through main-chain−main-chain and side-chain−side-chain interactions involving Phe4 of the inhibitor and Met81-Ala82-Gly83 of GpA70−86. This is fully consistent with the rational design of this inhibitor to target the GxxxG motif in GpA70−86 amyloid fibrils.[7] In addition to the side-chain–side-chain contact between Met81 and Phe4, we also find that two other side-chains of the inhibitor are important for recognition: Lys7 and Phe8 interacting with Val84 of the peptide (Figure 4B). Lys7 and Phe8 are therefore two positions for amino acid substitution and possible improvement of the binding free energy between GpA70−86 and the inhibitor.

Second, we find that there are multiple binding modes of the inhibitor to the GpA70−86 peptide. The predicted high preference for orthogonal orientation, followed by lower populated parallel and then antiparallel orientations of the $G_{79}VMAG_{83}$ peptide motif with respect to the G_2TFEG_6 inhibitor motif, does not run in contrast with the interaction site reported by Smith et al. based on sequence homology.[7] When experiments were run on the same inhibitor peptide binding to Aβ40, it was found that the inhibitor adopted both parallel and antiparallel orientations relative to Aβ GxMxG sequence.[38]

Third, on the basis of solid-state NMR experiments, Smith et al. proposed a parallel, in-register model for GpA70−86 fibril

with the peptides fully extended along with an inter-β-sheet distance of 0.3−0.5 nm and intrasheet distance of 0.8−1.0 nm between the carbonyl carbon of Gly79 and the methyl group of Met81.[7] These two solid-state NMR data do not rule out, however, the possibility of a peptide model having a β-hairpin with a turn at position Gly79 as predicted by our MD simulations of GpA70−86. This conformation has been observed or determined in the amyloid fibrils of the β2 m(20−41) peptide.[39,40] In addition, amide I FTIR spectra of the GpA70−86 peptides reconstituted with 1,2-dimyristoyl-*sn*-glycero-3-phosphocholine lipids show a peak at 1625 cm^{-1} probe of a β-sheet structure and a shoulder at 1657 cm^{-1} probe either of an α-helix[7] or a β-turn.[41] To determine whether the strand-loop-strand conformation is a possible building block in GpA70−86 fibril, we perform five independent 15-ns MD simulations at 310 K starting from a fibril model satisfying the two distances determined by solid-state NMR. The time evolution of the C_α-rmsd with respect to the initial state and the NMR distances in Figure 7 shows a rapid collapse, excluding the possibility that the fibril has a β-strand-loop-β-strand conformation of the peptides in vitro.

Finally, an important finding of this work is that the conformations sampled by the GxxxG motif of GpA70−86 do not vary much upon binding of the inhibitor. The predicted preference of the GxxxG motif for rather extended conformations is consistent with the suggestion that this motif mediates sheet-to-sheet packing.[7] Whether this conformational preference in GpA70−86 can be transferred to other amyloids and notably the two consecutive GxxxG motifs spanning Aβ29−37 remains to be determined, but this would simplify the conformations of Aβ40/42 during aggregation.

Acknowledgment. This work was supported by the National Natural Science Foundation of China (Grant No. 10674029) and program for New Century Excellent Talent in University (NCET-08-0125). H. Y. Li is thankful for the financial support from the Excellent Young Teacher Fund of Shanghai (Z-2008-25). P.D. acknowledges support from CNRS and a fellowship from Fudan University. Simulations were performed at the Réseau Québecois de Calcul de Haute Performance (with the support of Prof. Normand Mousseau) and the National High Performance Computing Center of Fudan University.

Supporting Information Available: Four figures reporting the MD-averaged secondary structure profile of GpA70−86 (Figure S1) and the inhibitor (Figure S2) in isolation and in the complex, the good sampling of the inhibitor around GpA70−86 (Figure S3), and the probability distribution of the peptide-inhibitor terminal C_α distances starting from three different GpA-inhibitor structures (Figure S4). This material is available free of charge via the Internet at http://pubs.acs.org.

References and Notes

(1) Sunde, M.; Serpell, L. C.; Bartlam, M.; Fraser, P. E.; Pepys, M. B.; Blake, C. C. *J. Mol. Biol.* **1997**, *273*, 729.

(2) Harmeier, A.; Wozny, C.; Rost, B. R.; Munter, L. M.; Hua, H.; Georgiev, O.; Beyermann, M.; Hildebrand, P. W.; Weise, C.; Schaffner, W.; Schmitz, D.; Multhaup, G. *J. Neurosci.* **2009**, *29*, 7582.

(3) Munter, L. M.; Voigt, P.; Harmeier, A.; Kaden, D.; Gottschalk, K. E.; Weise, C.; Pipkorn, R.; Schaefer, M.; Langosch, D.; Multhaup, G. *EMBO J.* **2007**, *26*, 1702.

(4) Hegde, R. S.; Mastrianni, J. A.; Scott, M. R.; DeFea, K. A.; Tremblay, P.; Torchia, M.; DeArmond, S. J.; Prusiner, S. B.; Lingappa, V. R. *Science* **1998**, *279*, 827.

(5) Florio, T.; Paludi, D.; Villa, V.; Principe, D. R.; Corsaro, A.; Millo, E.; Damonte, G.; D'Arrigo, C.; Russo, C.; Schettini, G.; Aceto, A. *J. Neurochem.* **2003**, *85*, 62.

(6) Der-Sarkissian, A.; Jao, C. C.; Chen, J.; Langen, R. *J. Biol. Chem.* **2003**, *278*, 37530.

(7) Liu, W.; Crocker, E.; Zhang, W.; Elliott, J. I.; Luy, B.; Li, H.; Aimoto, S.; Smith, S. O. *Biochemistry* **2005**, *44*, 3591.

(8) Antzutkin, O. N.; Balbach, J. J.; Leapman, R. D.; Rizzo, N. W.; Reed, J.; Tycko, R. *Proc. Natl. Acad. Sci. U. S. A.* **2000**, *97*, 13045.

(9) Luhrs, T.; Ritter, C.; Adrian, M.; Riek-Loher, D.; Bohrmann, B.; Dobeli, H.; Schubert, D.; Riek, R. *Proc. Natl. Acad. Sci. U. S. A.* **2005**, *102*, 17342.

(10) Ferguson, N.; Becker, J.; Tidow, H.; Tremmel, S.; Sharpe, T. D.; Krause, G.; Flinders, J.; Petrovich, M.; Berriman, J.; Oschkinat, H.; Fersht, A. R. *Proc. Natl. Acad. Sci. U. S. A.* **2006**, *103*, 16248.

(11) Derreumaux, P.; Mousseau, N. *J. Chem. Phys.* **2007**, *126*, 025101.

(12) Song, W.; Wei, G.; Mousseau, N.; Derreumaux, P. *J. Phys. Chem. B* **2008**, *112*, 4410.

(13) Lindahl, E.; Hess, B.; van der Spoel, D. *J. Mol. Model.* **2001**, *7*, 306.

(14) Van Gunsteren, W. F.; Billeter, S. R.; Eising, A. A.; Hunenberger, P. H.; Kruger, P.; Mark, A. E.; Scott, W. R. P.; Tironi, I. G. Biomolecular Simulation: The GROMOS96 Manual and User Guide; Vdf Hochschulverland, ETH, Zurich, Switzerland, 1996.

(15) Berendsen, H. J. C.; Postma, J. P. M.; Gunsteren, W. F. v.; Hermans, J. *Intermolecular Forces, Interaction Models for Water in Relation to Protein Hydration*; D. Reidel Publishing Company: Dordrecht, 1981.

(16) Hess, B.; Bekker, H.; Berendsen, H. J. C.; Fraaije, J. G. E. M. *J. Comput. Chem.* **1997**, *18*, 1463.

(17) Miyamoto, S.; Kollman, P. A. *J. Comput. Chem.* **1992**, *13*, 952.

(18) Berendsen, H. J. C.; Postma, J. P. M.; Gunsteren, W. F. v.; DiNola, A.; Haak, J. R. *J. Chem. Phys.* **1984**, *81*, 3684.

(19) MacKenzie, K. R.; Prestegard, J. H.; Engelman, D. M. *Science* **1997**, *276*, 131.

(20) Kabsch, W.; Sander, C. *Biopolymers* **1983**, *22*, 2577.

(21) Huet, A.; Derreumaux, P. *Biophys. J.* **2006**, *91*, 3829.

(22) Humphrey, W.; Dalke, A.; Schulten, K. *J. Mol. Graph.* **1996**, *14*, 33.

(23) Unterreitmeier, S.; Fuchs, A.; Schaffler, T.; Heym, R. G.; Frishman, D.; Langosch, D. *J. Mol. Biol.* **2007**, *374*, 705.

(24) Russ, W. P.; Engelman, D. M. *J. Mol. Biol.* **2000**, *296*, 911.

(25) Senes, A.; Gerstein, M.; Engelman, D. M. *J. Mol. Biol.* **2000**, *296*, 921.

(26) Melnyk, R. A.; Kim, S.; Curran, A. R.; Engelman, D. M.; Bowie, J. U.; Deber, C. M. *J. Biol. Chem.* **2004**, *279*, 16591.

(27) Cuthbertson, J. M.; Bond, P. J.; Sansom, M. S. *Biochemistry* **2006**, *45*, 14298.

(28) Efremov, R. G.; Vereshaga, Y. A.; Volynsky, P. E.; Nolde, D. E.; Arseniev, A. S. *J. Comput.-Aided Mol. Des.* **2006**, *20*, 27.

(29) Gervais, C.; Wust, T.; Landau, D. P.; Xu, Y. *J. Chem. Phys.* **2009**, *130*, 215106.

(30) Bond, P. J.; Wee, C. L.; Sansom, M. S. *Biochemistry* **2008**, *47*, 11321.

(31) Soto, P.; Griffin, M. A.; Shea, J. E. *Biophys. J.* **2007**, *93*, 3015.

(32) Chebaro, Y.; Derreumaux, P. *Proteins* **2009**, *75*, 442.

(33) Esteras-Chopo, A.; Morra, G.; Moroni, E.; Serrano, L.; Lopez de la Paz, M.; Colombo, G. *J. Mol. Biol.* **2008**, *383*, 266.

(34) Wu, C.; Wang, Z.; Lei, H.; Zhang, W.; Duan, Y. *J. Am. Chem. Soc.* **2007**, *129*, 1225.

(35) Yoda, T.; Sugita, Y.; Okamoto, Y. *Chem. Phys. Lett.* **2004**, *386*, 460.

(36) Wei, G.; Shea, J.-E. *Biophys. J.* **2006**, *91*, 1638.

(37) Baumketner, A.; Shea, J.-E. *J. Mol. Biol.* **2007**, *366*, 275.

(38) Sato, T.; Kienlen-Campard, P.; Ahmed, M.; Liu, W.; Li, H.; Elliott, J. I.; Aimoto, S.; Constantinescu, S. N.; Octave, J. N.; Smith, S. O. *Biochemistry* **2006**, *45*, 5503.

(39) Iwata, K.; Fujiwara, T.; Matsuki, Y.; Akutsu, H.; Takahashi, S.; Naiki, H.; Goto, Y. *Proc. Natl. Acad. Sci. U. S. A.* **2006**, *103*, 18119.

(40) Liang, C.; Derreumaux, P.; Mousseau, N.; Wei, G. *Biophys. J.* **2008**, *95*, 510.

(41) Derreumaux, P.; Vergoten, G. *J. Chem. Phys.* **1995**, *102*, 8586.

JP908889Q